Angiogenesis (2021) 24:583–595
https://doi.org/10.1007/s10456-021-09770-0

ORIGINAL PAPER

7-ketocholesterol induces endothelial-mesenchymal transition and promotes fibrosis: implications in neovascular age-related macular degeneration and treatment

Haibo Wang[1] · Aniket Ramshekar[1] · Eric Kunz[1] · M. Elizabeth Hartnett[1]

Received: 22 December 2020 / Accepted: 30 January 2021 / Published online: 28 February 2021

Abstract

Oxidized cholesterols and lipids accumulate in Bruch's membrane in age-related macular degeneration (AMD). It remains unknown what causal relationship exists between these substances and AMD pathophysiology. We addressed the hypothesis that a prevalent form, 7-ketocholesterol (7KC), promotes choroidal endothelial cell (CEC) migration and macular neovascularization in AMD. Compared to control, 7KC injection caused 40% larger lectin-stained lesions, but 70% larger lesions measured by optical coherence tomography one week after laser-injury. At two weeks, 7KC-injected eyes had 86% larger alpha smooth muscle actin (αSMA)-labeled lesions and more collagen-labeling than control. There was no difference in cell death. 7KC-treated RPE/choroids had increased αSMA but decreased VE-cadherin. Compared to control-treated CECs, 7KC unexpectedly reduced endothelial VE-cadherin, CD31 and VEGFR2 and increased αSMA, fibroblast activation protein (FAP) and transforming growth factor beta (TGFβ). Inhibition of TGFβ receptor-mediated signaling by SB431542 abrogated 7KC-induced loss of endothelial and increase in mesenchymal proteins in association with decreased transcription factor, SMAD3. Knockdown of SMAD3 partially inhibited 7KC-mediated loss of endothelial proteins and increase in αSMA and FAP. Compared to control, 7KC-treatment of CECs increased Rac1GTP and migration, and both were inhibited by the Rac1 inhibitor; however, CECs treated with 7KC had reduced tube formation. These findings suggest that 7KC, which increases in AMD and with age, induces mesenchymal transition in CECs making them invasive and migratory, and causing fibrosis in macular neovascularization. Further studies to interfere with this process may reduce fibrosis and improve responsiveness to anti-VEGF treatment in non-responsive macular neovascularization in AMD.

Keywords Age-related macular degeneration · 7-ketocholesterol · Choroidal endothelial cells · Endothelial-mesenchymal transition · Non-responsive (or unresponsive) neovascular AMD · Macular fibrosis

Introduction

Age-related macular degeneration (AMD) is a complex disease and a leading cause of vision loss world-wide [1, 2]. Outcomes have been revolutionized with the use of agents that interfere with the bioactivity of vascular endothelial growth factor (VEGF); however, only about 50% of eyes respond with long-term improved vision largely due to progression to macular atrophy or fibrosis [3–5]. Part of the complexity of AMD may relate to its strong association with genetic variants, [6, 7] and late manifestation in life. A number of studies have investigated external factors related to AMD [8, 9]. Some associated risk factors involve lifestyle, whereas others relate to age- and AMD-related changes in Bruch's membrane [10–12].

We have been interested in mechanisms that activate choroidal endothelial cells (CECs) to migrate into the neural retina, an event that causes vision loss in type 2 macular neovascularization (type 2 MNV) in AMD [13]. To explore mechanisms of CEC activation and migration, we have used physiologically relevant human cell cultures to study various stresses involved in AMD pathophysiology. We found that activation of the Rac1, a small GTPase protein, increased CEC migration [14], and that several AMD-related stresses activated Rac1, including inflammatory cytokines, e.g., tumor necrosis factor alpha (TNFα) [15]; angiogenic

✉ M. Elizabeth Hartnett
ME.Hartnett@hsc.utah.edu

[1] The John A Moran Eye Center, University of Utah, 65 Mario Capecchi Drive, Salt Lake City, UT, USA

factors, VEGF [16, 17] and C-C motif chemokine 11 [18, 19]; and reactive oxygen species generated by NADPH oxidase [2]. In this study, we explored the role of extracellular deposits that accumulate in Bruch's membrane with increased age [20] and in AMD [21, 22]. These deposits and drusen are composed of a number of substances, including complement, proteins, cholesterol and oxysterols. A prevalent oxysterol in Bruch's membrane and drusen in AMD is 7-ketocholesterol (7KC) [22, 23], which is synthesized in the retina [24] or can form from non-enzymatic oxidation of blood-borne lipids and cholesterol [25, 26]. 7KC is cytotoxic [20], but nontoxic effects involve pathways of inflammation, oxidation [27], and angiogenesis including through VEGF [28]. 7KC is also the predominant oxysterol in the blood of patients with cardiovascular disease [29], an associated risk of AMD [20].

We proposed the hypothesis that 7KC in the blood stream and Bruch's membrane would have access to and activate CECs to become migratory and form MNV. We addressed this hypothesis using experimental methods with isolated human CECs and in mice treated with laser-injury to induce choroidal neovascularization (CNV). As predicted, we found 7KC activated Rac1 in CECs and increased CNV induced by laser injury. Unexpectedly, we found 7KC also reduced the expression of endothelial markers on CECs and increased the expression of mesenchymal markers. We, therefore, refined our studies to address the predictions that 7KC induces endothelial-mesenchymal transition (EndMT) and increases migratory invasiveness of the transitioned cells, leading to enlarged lesions and fibrosis. We provide evidence that 7KC induces EndMT of CECs and leads to aggressive migratory characteristics and invasion that lead to fibrosis in an experimental model of neovascular AMD. The transitioned cells lack VEGFR2, and this may render them poorly responsive to anti-VEGF treatment.

Materials and methods

Animals and ethical statement

Wild type C57Bl/6J mice purchased from Jackson Laboratory (Bar Harbor, ME) were used in this study. All the experimental procedures were approved by Institutional Animal Care and Use Committee and the Institutional Biosafety Committee of Utah, and followed the Guide for the Care and Use of Laboratory Animals of the University of Utah and the Association for Research in Vision and Ophthalmology Statement for the Use of Animals in Ophthalmic and Vision Research. Inhalation of isoflurane (Millipore Sigma, St. Louis, MO) and intraperitoneal injections of Ketamine (90 mg/Kg) and Xylazine (10 mg/Kg) for anesthesia, and cervical dislocation was used for euthanasia under anesthesia.

Intravitreal injections of 7KC, laser-induced CNV model and optical coherence tomography

Six-week-old mice received bilateral intravitreal injections of 7KC (1 µl of 5 µM 7KC/eye) or the vehicle control, 2-Hydroxypropyl-β-cyclodextrin (HPBCD, Sigma-Aldrich). One-week post injection, mice were then treated with laser using the Phoenix Image-Guided Laser System 94 (Phoenix Micron IV, Pleasanton, CA). As described previously [30], following dilation with 1% tropicamide ophthalmic solution and pain control with 0.5% proparacaine hydrochloride Ophthalmic solution (California Pet Pharmacy, Hayward, CA), mice were treated with laser at settings of 460 mW intensity and 100 ms duration to induce CNV. Each eye received four laser spots that were located at approximately two disc diameters from the optic nerve. Right after laser, mice received the second intravitreal 7KC or HPBCD injections through a site separate from the previous site. Lesion volumes were measured by spectral domain optical coherence tomography (OCT) at one week post laser under anesthesia as described previously [31]. One week or two weeks after laser, mice were euthanized and eyes were collected for RPE/choroidal flatmounts for lesion volume or protein analysis.

RPE/choroidal flat mount preparation, staining, and lesion volume quantification

Fresh enucleated eyes were first fixed in 4% paraformaldehyde (Electron Microscopy Sciences, Hatfield, PA) for 1 h and followed by an additional 1 h after removing the cornea, lens, vitreous and retina. The posterior eyecups were then blocked in phosphate-buffered saline (PBS) containing 1% bovine serum albumin (BSA) and 0.5% Triton X-100 at room temperature, and followed by staining with AlexaFluor 568-conjugated Isolectin B4 (1:500, Invitrogen, Carlsbad, CA), and alpha smooth muscle actin (αSMA) (1:200, Cell Signaling Technology, Danvers, MA) overnight at 4 °C. To label αSMA staining, the eyecups were stained with FITC-conjugated goat anti-Rabbit secondary antibody (1:200, Invitrogen, Carlsbad, CA) for 1 h at room temperature. After three washes, the eyecups were flattened by cutting incisions radially and mounted onto a microscope slide with VECTASHIELD mounting medium (Vector Laboratories, Burlingame, CA).

Confocal images of each lectin or αSMA-labeled lesion with the z-stack set at 1 nm intervals were captured at 488 and 568 nm using a 20X objective on a Confocal Laser Scanning Microscope (Olympus Corporation, Japan).

Images were imported into IMARIS (the Oxford Instruments, Switzerland), and lesion volumes were determined using the Surfaces Module (Version 9.1.2, Bitplane, Santa Barbara, California, USA). Lesions with obvious hemorrhage or bridging CNV were excluded.

Immunostaining in mouse retinal cryosections

For staining in retinal cryosections, eyes were first fixed in 4% paraformaldehyde for 1 h and an additional 1 h after removing the cornea and lens. Eyecups were then dehydrated in 15% sucrose for 2 h at room temperature, followed by 30% sucrose overnight at 4 °C, and embedded in optimal cutting temperature (OCT) (Tissue Tek, Hatfield, PA). The frozen OCT-embedded tissues were sectioned into 12 µm sections using a cryotome cryostat (ThermoFisher Scientific). After blocking in 5% normal goat serum in PBS/0.3% Triton X-100 for 1 h at room temperature, cryosections were then incubated with rabbit anti-collagen I (1:150, Thermofisher Scientific) overnight at 4 °C and followed by 1 h incubation at room temperature with Cyanine Cy^{TM}3-conjugated goat anti-rabbit IgG antibody (1:200, Jackson ImmunoResearch Lab, West Gove, PA) with isolectin B4-488 (1:500, Invitrogen) and TO-PRO-3 (1:500, ThermoFisher Scientific, Waltham, MA) to stain CNV lesions and nuclei, respectively. Sections were then washed in PBS for three times and mounted in Fluoromount-G (SouthernBiotech, Birmingham, AL). Images were captured using a confocal microscope (FV1000, Olympus, Japan). The integrated density of collagen I at the CNV lesions was quantified using Image J (developed by National Institute of Health of the United States, USA).

TUNEL staining in retinal cryosections

TUNEL staining was performed using the In Situ Cell Death Detection Kit-TMR red (Roche Diagnostics GmbH, Mannheim, Germany). Following instructions in the kit, sections were washed in PBS (pH 7.4) and incubated in freshly prepared permeabilization solution (0.1% Triton X-100 in 0.1% sodium citrate). After two rinses with PBS, sections were incubated with the TUNEL reaction mixture (50 µl Enzyme solution to 450 µl Label solution) for 1 h at 37 °C. Sections pre-incubated with DNase I recombinant (3000 U/ml–3 U/ml in 50 mM Tris-HCl, pH 7.5, 1 mg/ml BSA) for 10 min at room temperature were used as positive controls. Sections incubated with only the Label solution were used as negative controls. After three rinses in PBS for 5 min each, coverslips were mounted in DAPI-Fluoromount-G (SouthernBiotech, Birmingham, AL). TUNEL positive cells were detected under a confocal microscope (FV1000, Olympus, Japan) at 580 nM.

Cell culture, siRNA transfection and treatment

Human choroidal endothelial cells (CECs) were isolated from human donor eyes (20–40 years of age) (Utah Lions Eye Bank, Salt Lake City, UT). Human Subjects Committee of University of Utah deemed our use of de-identified donor eyes to isolate human CECs was exempt. Experiments were replicated in CECs from three different donors. As described previously [30], CECs at passages 2–5 were grown in Endothelial Growth Medium (EGM2; Lonza, Walkersville, MD) with 5% fetal bovine serum (FBS).

To knock down SMAD3, CECs at 80% confluence were transfected with siRNA targeting human *SMAD3* gene or silencer selective control siRNA (Applied Biosystems, Foster City, CA).

For treatment, CECs in EGM2 were treated with 7KC (10 µM, Cayman Chemical, Ann Arbor, Michigan) or tumor growth factor beta (TGFβ) (10ng/ml, R&D Systems, Minneapolis, MN), or respective solvent control, 45% (2-Hydroxypropyl)-β-cyclodextrin (HPBCD, Sigma-Aldrich) or PBS. Some CECs were pretreated with a TGFβ receptor inhibitor, SB431542 (10 µM, Selleckchem, Pittsburgh, PA), Rac1 inhibitor (50 µM, MilliporeSigma, Burlington, MA) or vehicle control.

Rac1 activity assay by immunoprecipitation

After treatment, CECs were collected and lysed in radioimmunoprecipitation assay (RIPA) buffer (50 mM Tris pH 7.4, 150 mM sodium chloride, 0.5% sodium deoxycholate, 0.1% sodium dodecyl sulfate, 1% Triton X-100 and 10% glycerol) with protease inhibitors (Roche Diagnostics, Indianapolis, IN) and phosphatase inhibitors (Thermo Scientific, Rochford, IL). The protein concentration in cell lysate was quantified using Bicinchoninic acid assay kit (Thermo Scientific). Three hundreds microlitters of cell lysates containing 300 µg of protein were processed for immunoprecipitation (IP) with an antibody to Rac1GTP (1:100; NewEast Biosciences, King of Prussia, PA) by gently rocking at 4 °C. The antibody/protein complex was pulled down with 10 µl of Dynabeads protein G (Invotrogen, Carlsbad, CA) and re-suspended in 2X sample buffer (ThermoFisher Scientific) after three washes in RIPA buffer. Rac1GTP in the IP products were measured by Western blots using an antibody to Rac1 (BD Transduction Laboratories, Franklin Lakes, NJ).

Western blots

After quantitation of protein concentration, 10–20 µg protein from cells and tissues was separated by NuPAGE 4% to

12% Bis-Tris Gels (Invitrogen) and transferred to a PVDF membrane using iBlot 2 Gel Transfer Device (ThermoFisher Scientific). The PVDF membranes were first blocked in tris-buffered saline (TBS) (Quality Biological, Gainthersburg, MD) blocking buffer with 5% BSA for 1 h at room temperature and then incubated with antibodies to vascular endothelial growth factor receptor 2 (VEGFR2), CD31, vascular endothelial cadherin (VE-cadherin), αSMA, TGFβ, SNAIL (Cell signaling Technology, Danvers, MA) or fibroblast activation protein (FAP) (abcam, Cambridge, MA) overnight at 4ºC. The membranes were reprobed with HRP-conjugated β-actin (Santa Cruz Biotechnology, Dallas, Texas) as loading controls. Densitometry analysis was performed with the use of the software UN-SCAN-IT version 7.1 (Silk Scientific, Orem, UT).

Transwell cell migration and tube formation assays

Migration assays similar to what we previously developed [14] for retinal pigment epithelium and CECs but fashioned after Boyden assays for CECs were performed in 24-well plates with 6.5 mm diameter Transwell inserts (8 µm pores; Corning, NY). After 72 h treatment with 7KC or HPBCD in the presence of the Rac1 inhibitor or PBS control, CECs were stained with Vybrant DiO (Invitrogen, Carlsbad, CA) for 10 min at 37 °C, and seeded into the inserts at 50,000 cells in 200 µl of EGM2 media. Five hundred microlitters of EGM2 were added into each well beneath the insert. The plates were allowed to incubate at 37 °C, 5% CO_2. The cells that had not migrated and were still located in the inserts were carefully removed using cotton tips, and the inserts were then fixed in 4% paraformaldehyde. The cells that had migrated to the underside of the insert were imaged with a confocal microscope (FV1000, Olympus, Japan) and quantified by two masked reviewers.

For the tube formation assay, growth factor-reduced Matrigel (Corning, New York), thawed overnight, was plated onto 48-well plates and incubated for 30 min at 37 °C to solidify. After 72 h treatment with 7KC or HPBCD, CECs in EBM-2 were seeded on top of Matrigel at 40,000 cells/well. After 12 h of incubation, tubes were imaged using phase-contrast on a BZ-X810 fluorescent microscope (Keyence, Itaska, IL) at 10× magnification. Images were imported into FIJI software and tube cavitations were quantified.

Statistical analysis

The statistical significance of CNV lesions was analyzed with a mixed effects linear regression model using STATA-14 software (StataCorp LLC, College Station, TX). The model included both fixed and random effects to account for biological variation between litters by comparing experimental to control groups. In general, one eye from each animal was used for the analysis of lesions, and the fellow eye was used for protein analysis. *A* two-tailed t-test was used to determine the difference in protein from tissues and cells. A statistical significance was determined when the *P* value was < 0.05. For animal studies, at least 33 CNV spots from at least 11 animals were included. For immunolabeled cryosections, 3–4 sections at 60 µm intervals were taken from one eye, and a total of two eyes from different animals were included in each group. For protein analyses, each treatment included at least six different animals from 3 litters. For in vitro studies, each experimental condition included an $n = 3–6$ from at least two independent experiments, and CECs from three different donor eyes were included. Results were presented as Mean ± SEM or SD as indicated in Figure legends.

Results

7KC Increases CNV lesions in a laser-induced model

We postulated that 7KC, which activated pro-inflammatory and oxidative signaling in the ECs in other models [28, 32], would activate CECs to migrate and increase laser-induced CNV. We tested this prediction by injecting 7KC or control HPBCD into the vitreous of both eyes of 6-week-old wild type C57Bl/6J mice and, one week later, treated the eyes with laser and additional bilateral intravitreal injections of 7KC or HPBCD. CNV volumes were measured by OCT and lectin-stained RPE/choroidal flat mounts 7 days after laser. Compared to HPBCD-treated mice, those that received intravitreal 7KC had 1.44-fold larger CNV volumes measured on lectin-labeled flat mounts (Fig. 1a and b). However, volumes measured from OCTs were 1.8-fold greater in 7KC-treated vs. HPBCD-treated eyes (Fig. 1c and d).

7KC increases fibrosis of laser-induced lesions without inducing cell death

To address possible causes for the fold differences between OCT and lectin-labeled CNV lesions in 7KC- vs. HPBCD-treated eyes, we colabeled choroidal flat mounts with different markers, lectin, αSMA or collagen 1, which have been reported in MNV [33]. We found αSMA surrounded lectin-stained lesions (Fig. 2a). The volumes of lesions stained by αSMA in 7KC-treated eyes were significantly greater than in HPBCD-treated eyes (Fig. 2b) two weeks after laser. There was also a pattern of increased collagen 1 labeling in 7KC-treated eyes ($p = 0.08$) at two weeks (Fig. 2c, d). (Collagen I staining was not detected in sections incubated with only secondary antibody (non-primary control, Supplemental Fig. 1a)). Taken together, these findings suggest that 7KC increases fibrosis in laser-induced CNV lesions.

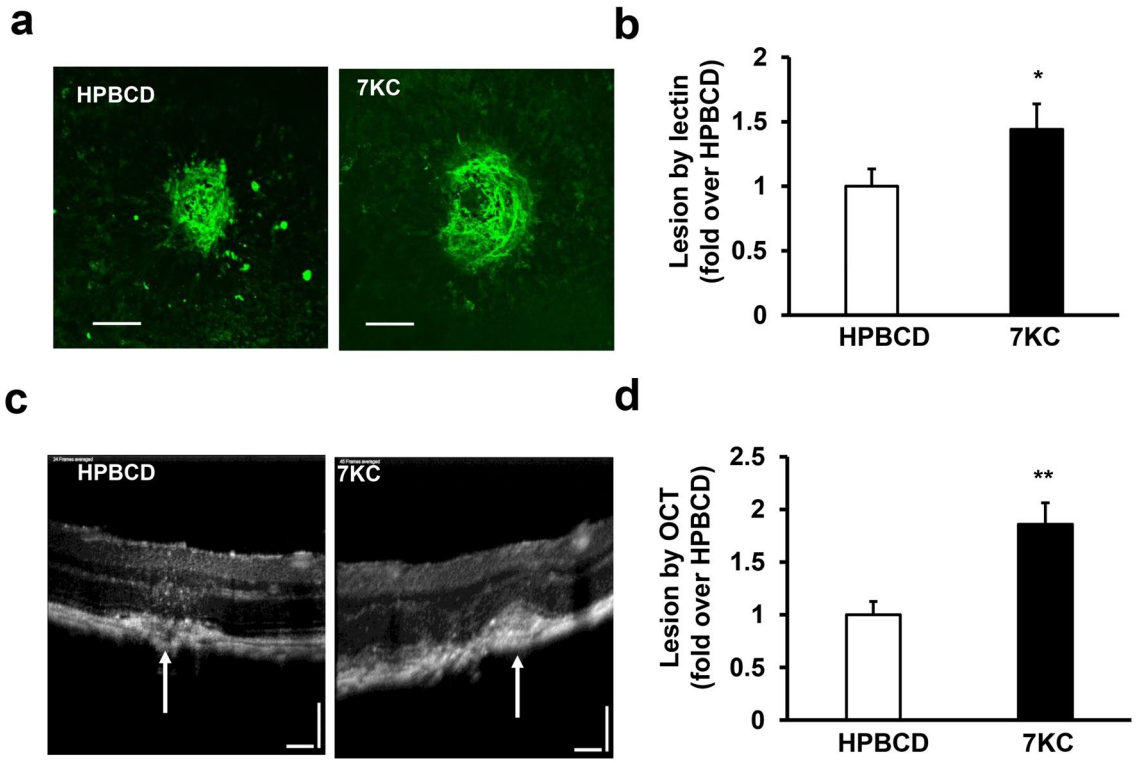

Fig. 1 Intravitreal injections of 7KC increase CNV lesion in a laser-induced CNV model. **a** Representative images of RPE/choroidal flat mounts stained with lectin (scale bar: 100 µm), **b** fold increase in lectin-stained CNV volume; **c** representative OCT images lesions and **d** fold increase in lesion volume measured by OCT in wild type mice one week post laser treatment (*p < 0.05, **p < 0.01 vs. HPBCD; Results were Mean ± SEM)

7KC can be toxic [20]. To determine if 7KC treatment increased cell death in the retina, TUNEL staining was performed in retinal cryosections of eyes treated with 7KC or HPBCD two weeks after laser. Compared to HPBCD, 7KC treatment did not increase TUNEL positive cells in the retina treated with laser (Fig. 3), suggesting that 7KC did not lead to increased cell death. (Sections incubated only with Label Solution without Enzyme Solution were used as negative controls and sections pre-incubated with DNase I recombinant (3U/ml) for 10 min prior to incubation with TUNEL reaction mixture were used as positive controls (Supplemental Fig. 1b)).

7KC promotes choroidal endothelial mesenchymal transition

We then quantified mesenchymal cell markers, αSMA and FAP and endothelial markers, VE-cadherin and VEGFR2 in RPE/choroids 7 days after laser from 7KC- and HPBCD-treated mice. Compared to HPBCD, αSMA (Fig. 4a) and FAP (Fig. 4b) were significantly increased in RPE/choroids of 7KC-treated eyes, and VE-cadherin was significantly decreased in the same tissue lysates (Fig. 4c). VEGFR2 also tended to be reduced in 7KC-treated compared to HPBCD-treated (p=0.175 vs. HPBCD, Fig. 4d). These findings support the hypothesis that 7KC increased mesenchymal transition.

In eyes, 7KC might affect mesenchymal transition and fibrosis by recruiting mesenchymal cells or fibroblasts, or as reported in cancer and cardiovascular disease, 7KC might affect signaling mechanisms in endothelial or epithelial cells to induce mesenchymal transition (EndMT or EMT, respectively) [34]. Given the loss of VE-cadherin, we tested the prediction that CECs were transitioning into mesenchymal cells after exposure to 7KC. We cultured CECs with 7KC or HPBCD and found that compared to HPBCD, CECs treated with 7KC for 48 or 72 h had significantly increased mesenchymal proteins, αSMA (Fig. 5a and b) and FAP (Fig. 5c and d), and increased TGFβ (Fig. 5e and f), which is a regulator of EMT and EndMT [34, 35]. However, in the same cell lysates, endothelial proteins, VEGFR2 (Fig. 6a and b), VE-cadherin (Fig. 6c and d) and CD31 (Fig. 6e and f), were significantly reduced in 7KC-treated compared to HPBCD-treated CECs. The findings provided further support that 7KC caused mesenchymal transition, specifically EndMT of CECs.

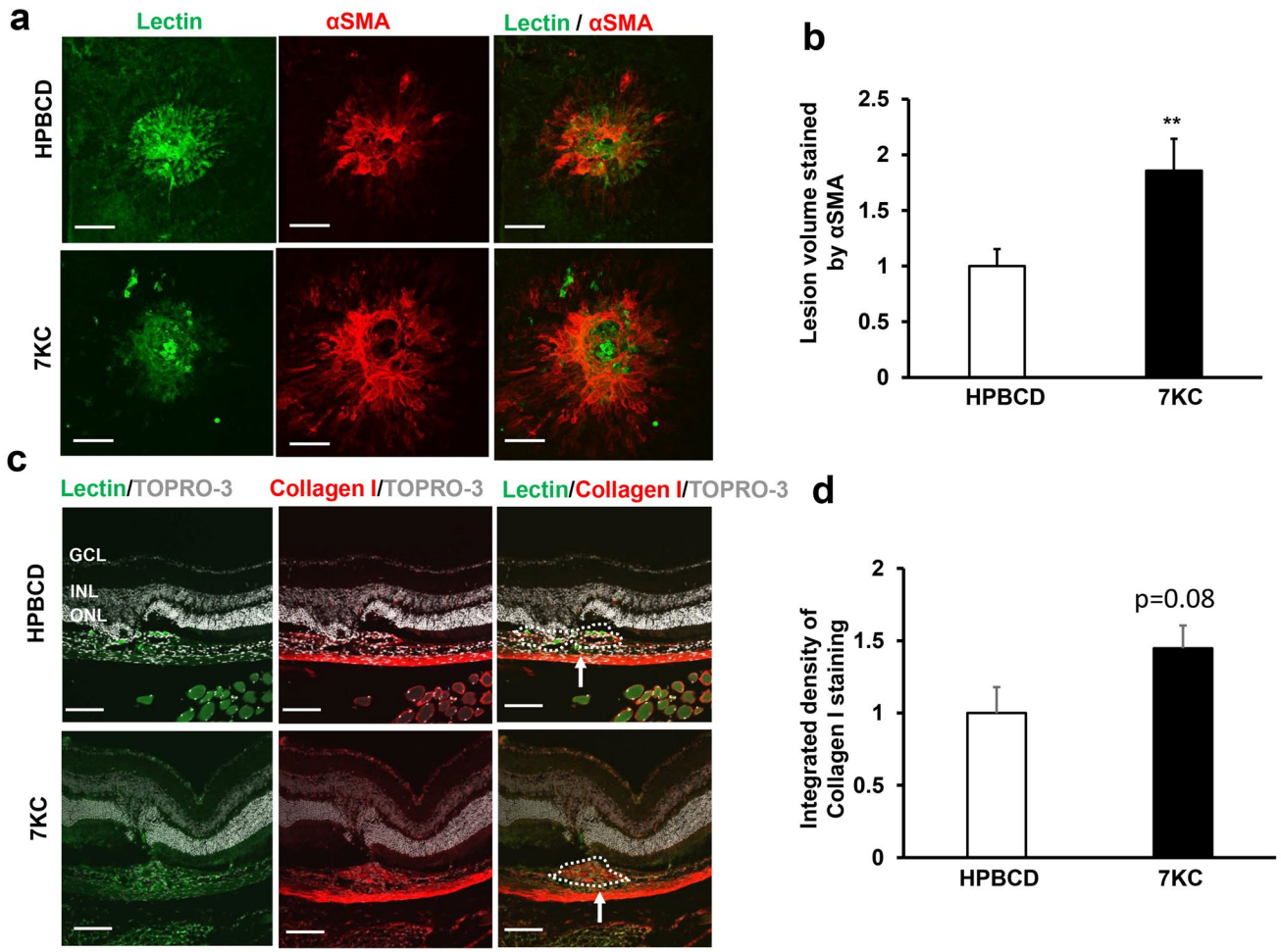

Fig. 2 Intravitreal injections of 7KC promote fibrosis of lesions induced by laser treatment. **a** Representative images of RPE/choroidal flat mounts stained by lectin and αSMA (Green: lectin; Red: αSMA; scale bar: 100 μm)) and **b** quantification of lesion volume stained by αSMA; **c** immunostaining of collagen I in retinal cryosections (scale bar: 100 μm) and **d** quantification of collagen I density at lesions of wild type mice 2 weeks post laser treatment (Green: lectin; Red: Collagen I; Gray: Topro3 to stain the nuclei; GCL, ganglion cell layer; INL, inner nuclear layer; ONL, outer nuclear layer; RPE, retinal pigment epithelium; the white arrows point to lesions; the areas labeled with dashed lines indicate the places where integrated density of collagen I was quantified) ($p = 0.08$, $^{**}p < 0.01$ vs. HPBCD; Results were Mean ± SEM)

7KC promotes EndMT via TGF β-dependent SMAD3 upregulation

The data in Figs. 4, 5, 6 provide evidence 7KC promotes EndMT of CECs and lesion fibrosis in mice, shown in Figs. 1 and 2. We, therefore, explored the mechanisms whereby 7KC mediated EndMT in CECs. TGFβ, which was upregulated by 7KC (Fig. 5e and f), is a well-studied growth factor that regulates EMT and EndMT [36, 37]. By binding its receptor, TGFβ receptor II, TGFβ transduces the signal to increase mesenchymal proteins. To gain insight into potential roles of TGFβ-mediated signaling in 7KC-induced CEC EndMT, CECs were incubated with TGFβ for 48 h and compared to CECs treated with 7KC, or respective controls. Similar to 7KC treatment, TGFβ treatment reduced VEGFR2, VE-cadherin and CD31 compared to PBS (Fig. 7a); however, in the same cell lysates, FAP, αSMA and TGFβ were increased (Fig. 7b). Outcomes were abrogated in CECs pretreated with the TGFβ receptor inhibitor, SB431542, for 30 min prior to incubation with 7KC or HPBCD (Figs. 7c and 7d). (SB431542 effectively blocked the effects of TGFβ in reducing VEGFR2 and in increasing TGFβ (Supplemental Fig. 2a)). These findings support the thinking that 7KC mediates EndMT of CEC through TGFβ-dependent signaling.

The process of TGFβ-mediated EndMT is tightly regulated by the transcription factors, including the SMADs [38]. To determine if SMAD was involved in 7KC-mediated EndMT of CECs, SMAD2/3 were measured by western blots using an antibody to recognize both SMAD2 and SMAD3 in CECs

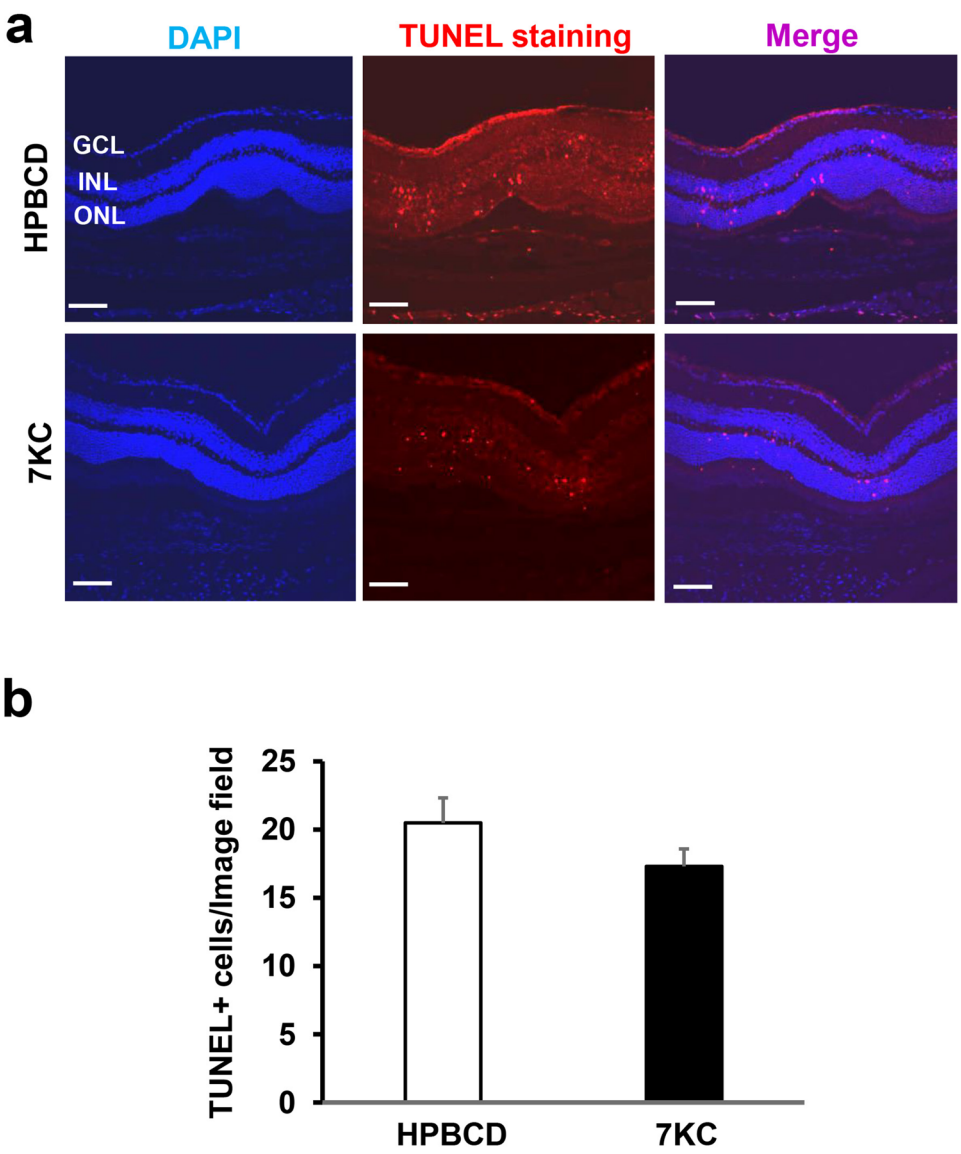

Fig. 3 Intravitreal injections of 7KC do not increase cell death determined by TUNEL staining in the retina of wild type mice two weeks post laser treatment. **a** Representative images of TUNEL staining in retinal cryosections (Red: TUNEL positive cells; Blue: DAPI to stain the nuclei; scale bar: 100 µm) and **b** quantification of TUNEL positive cells (Results were Mean ± SEM)

treated with 7KC. Compared to HPBCD, 7KC increased SMAD2/3 and pretreatment with SB431542 blocked 7KC-mediated SMAD2/3 upregulation (Fig. 8 a). To determine if SMAD2/3 was the transcriptional regulator for 7KC-mediated EndMT of CECs, we first tested EndMT in CECs transfected with *SMAD2*siRNA. We found that knockdown of SMAD2 did not affect 7KC-mediated EndMT of CECs (data now shown). We next measured VEGFR2, CD31, VE-cadherin, FAP and αSMA in CECs transfected with *SMAD3*siRNA to knockdown SMAD3 (Fig. 8b) and treated with 7KC or HPBCD for 72 h. In ControlsiRNA-transfected CECs, 7KC decreased VEGFR2, CD31 and VE-cadherin (Fig. 8c) and increased FAP and αSMA (Fig. 8d). 7KC-mediated loss of VEGFR2 and VE-cadherin was partially blocked in CECs knocked down for SMAD3 (Fig. 8c). Conversely, knockdown of SMAD3 inhibited both HPBCD- and 7KC-mediated induction of αSMA and FAP (Fig.8d). This finding suggests that SMAD3 upregulation is required for 7KC-mediated loss of endothelial proteins and induction in mesenchymal proteins.

EndMT of CECs shows increased migratory phenotypes via active Rac1

EndMT reported in cancer and cardiovascular disease leads to the transition of specialized endothelial cells to highly invasive mesenchymal cells [39, 40], which lose their function as endothelial cells. To determine if CECs that had undergone EndMT still maintain endothelial cell functions, we measured cell migration for invasive characteristics and tube formation, to assess endothelial function, after treatment with 7KC for 3 days. 7KC treatment activated Rac1 determined by increased Rac1GTP (Fig. 9a) and significantly increased cell migration (supplemental Fig. 2b and Fig. 9b) but did not increase tube

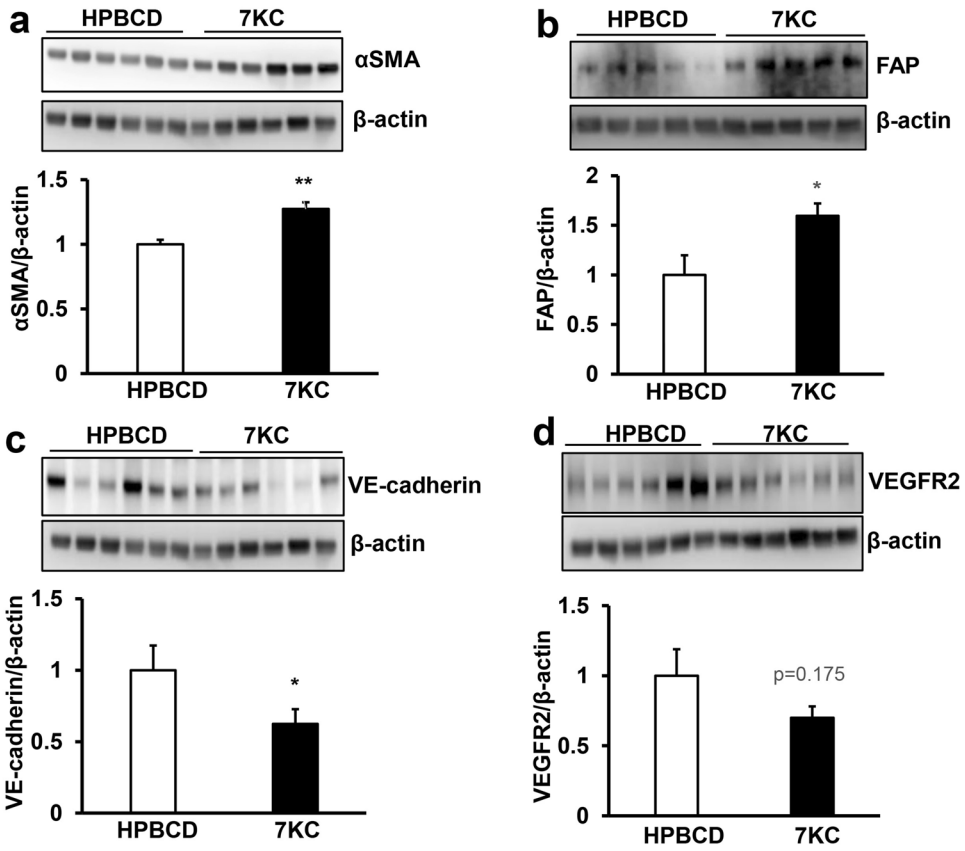

Fig. 4 Intravitreal injections of 7KC increase mesenchymal proteins and reduce endothelial proteins in the RPE/choroids from wild type mice one week after laser treatment. Western blots of **a** αSMA, **b** FAP, **c** VE-cadherin and **d** VEGFR2 (top panels: representative gel images; bottom panels: quantification of densitometry) ($p=0.175$, $^{*}p < 0.05$, $^{**}p < 0.01$ vs. HPBCD; Results were Mean ± SEM)

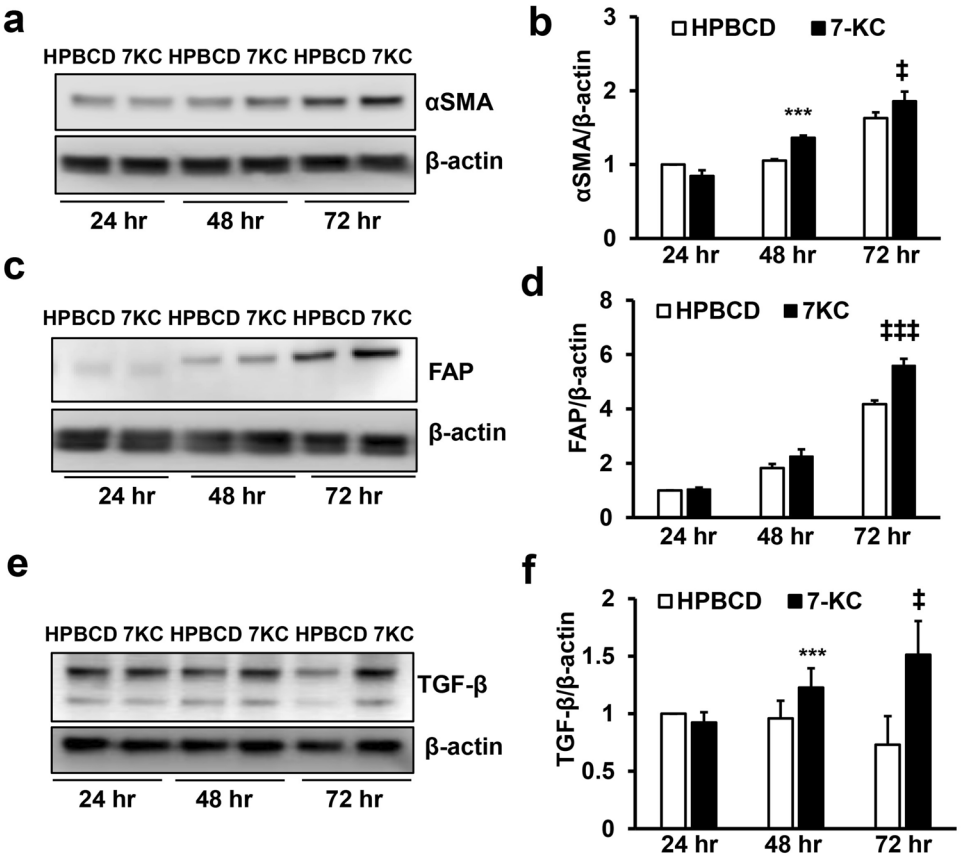

Fig. 5 7KC increases mesenchymal cell markers in choroidal endothelial cells (CECs). Western blots of (**a** and **b**) αSMA, (**c** and **d**) FAP and (**e** and **f**) TGFβ in CECs treated with 7KC or HPBCD for 24, 48 or 72 h (**a**, **c** and **e**: representative gel images; and **b**, **d** and **f**: quantification of densitometry) ($^{***}p < 0.001$ vs. HPBCD at 48 h; $^{‡}p < 0.05$ and $^{‡‡‡}p < 0.001$ vs. HPBCD at 72 h; Results were Mean ± SD)

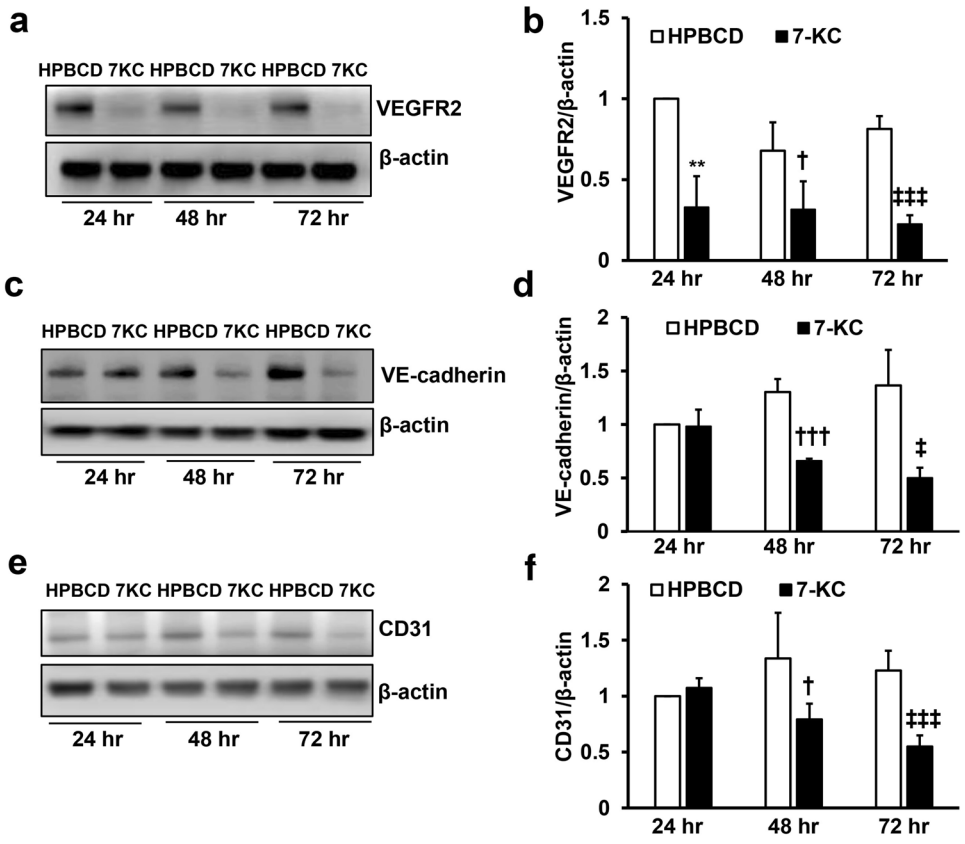

Fig. 6 7KC reduces endothelial cell markers in choroidal endothelial cells (CECs). Western blots of (**a** and **b**) VEGFR2, (**c** and **d**) VE-cadherin and (**e** and **f**) CD31 in CECs treated with 7KC or HPBCD for 24, 48 or 72 h (**a**, **c** and **e**: representative gel images and b, d and f: quantification of densitometry) (**p < 0.01 vs. HPBCD at 24 h; †p < 0.05 and †††p < 0.001 vs. HPBCD at 48 h and ‡p < 0.05 and ‡‡‡p < 0.001 vs. HPBCD at 72 h; Results were Mean ± SD)

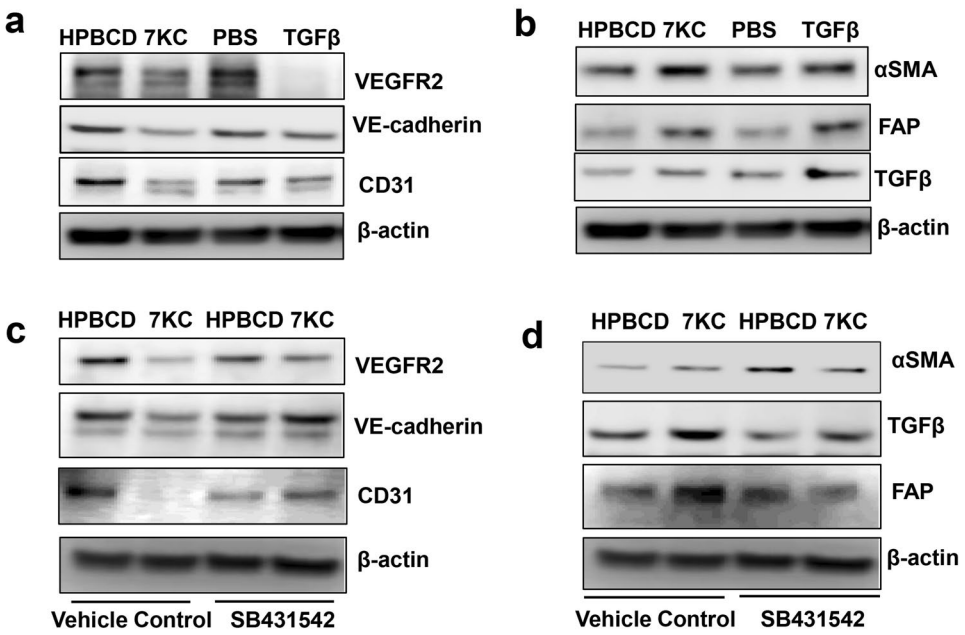

Fig. 7 7KC promotes EndMT of CECs via TGFβ-dependent signaling. Western blots of (**a**) VEGFR2, VE-cadherin and CD31 and (**b**) αSMA, FAP and TGFβ in CECs treated with 7KC or TGFβ or respective controls for 72 h; Western blots of (**c**) VEGFR2, VE-cadherin and CD31, and (**d**) αSMA, FAP and TGFβ in CECs in CECs pretreated with SB431541 and incubated with 7KC or HPBCD for 72 h.

formation (Fig. 9c and d). To determine if 7KC-mediated cell migration depended on activation of Rac1, CECs were pretreated with a Rac1 inhibitor 30 min to inhibit 7KC-mediated Rac1 activation (Fig. 9a) prior to incubation with 7KC or HPBCD. Compared to control, treatment with the Rac1 inhibitor significantly inhibited 7KC-mediated cell migration (Fig. 9b).

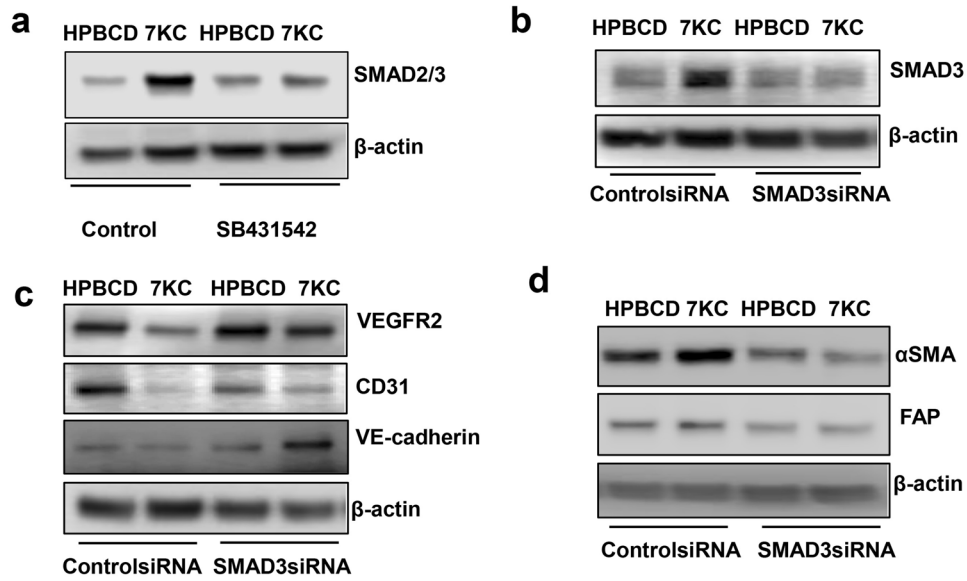

Fig. 8 Upregulation of SMAD3 is involved in 7KC-mediated EndMT of CECs. Western blots of (**a**) SMAD3 in CECs pretreated with control or SB431542 and treated with HPBCD or 7KC for 72 h, and (**b**) SMAD3 (**c**) VEGFR2, VE-cadherin and CD31, and (**d**) αSMA, FAP and TGFβ in CECs transfected with SMAD3 siRNA or ControlsiRNA and treated with 7KC for 72 h

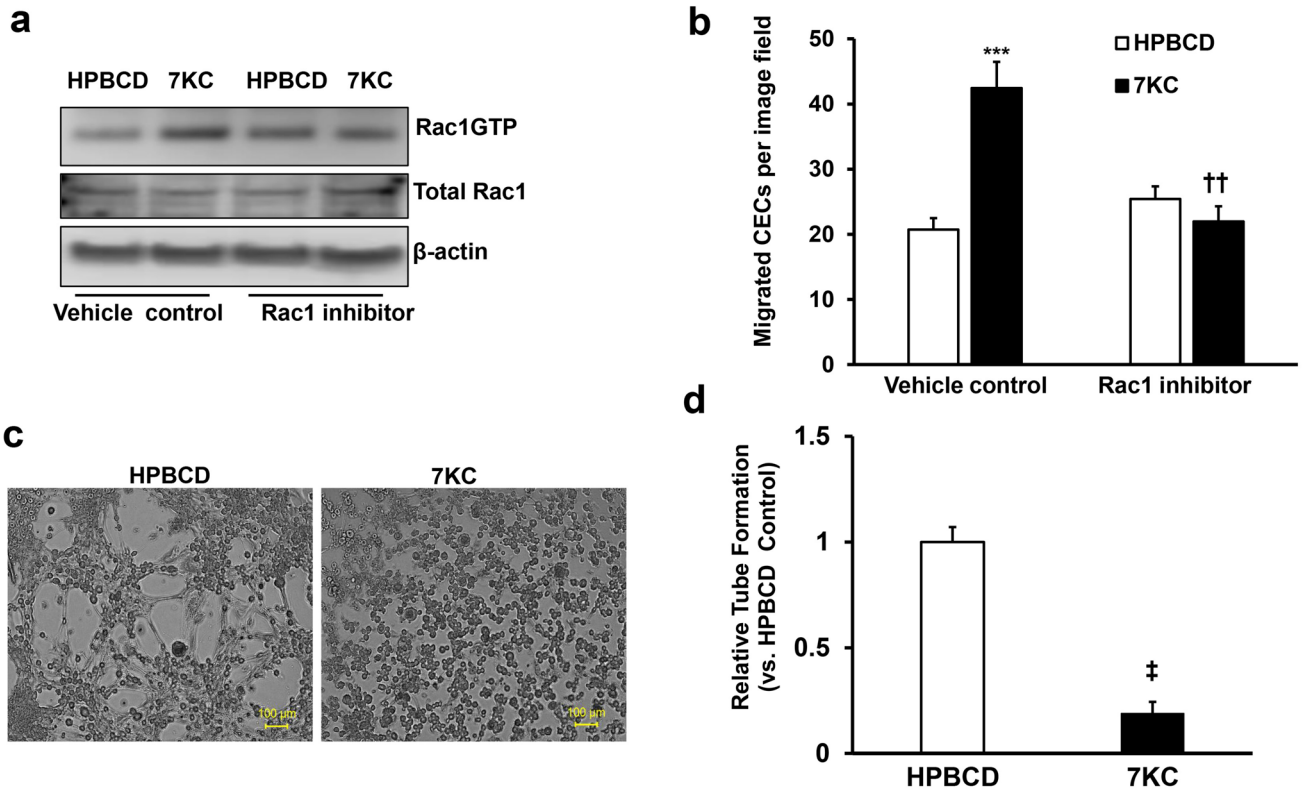

Fig. 9 7KC promotes cell migration via Rac1GTP dependent signaling, but does not induce tube formation. **a** Rac1 activity assay and **b** cell migration assay were performed in CECs after treatment with 7KC or HPBCD for 72 h in the presence of the Rac1 inhibitor or vehicle control (***$p < 0.001$ vs. HPBCD of Vehicle control; $^{\dagger\dagger}p < 0.01$ vs. 7KC of Vehicle control; Results were Mean ± SEM); (**c** and **d**) tube formation assay were performed in CECs treated with 7KC or HPBCD for 72 h (c, representative images of tube formation; ‡$p < 0.05$ vs. HPBCD; Results were Mean ± SD)

Discussion

Although anti-VEGF agents have revolutionized neovascular AMD management, only ~50% of patients have improved long-term vision and 50% respond minimally with progressive pathology from macular atrophy and fibrosis [3–5]. Understanding causes of non-responsive macular neovascularization are needed to improve outcomes in AMD. Our study is novel in that we identified mechanisms whereby 7KC induces EndMT and fibrosis, which may be a cause for non-responsive neovascular AMD to anti-VEGF agents, and is a leading cause of failed AMD treatment. Previous studies provide evidence of EMT of RPE cells and retinal EndMT in AMD [34, 41].

7KC, an oxidized form of cholesterol, accumulates in age and in diseases including cancer and heart disease. 7KC is the most predominant oxysterol in the serum with increasing age [20] and accumulates in Bruch's membrane and in drusen with increasing age and in AMD [22]. In this study, we tested the hypothesis that accumulation of 7KC mediates activation of CECs to transmigrate the RPE into the neural retina, become MNV and cause vision loss. In the murine laser-induced model, we unexpectedly found that intravitreal injections of 7KC not only significantly increased lectin-stained CNV volumes, but also increased αSMA-stained lesion and OCT-measured volumes to a greater extent than control. In laser-treated RPE/choroids, mesenchymal markers, αSMA and FAP, were increased and endothelial marker, VE-cadherin, reduced by 7KC. Although VEGFR2 was not significantly reduced by 7KC in RPE/choroids, it is possible that measured VEGFR2 expressed in other cells, such as the RPE, may have diluted the effect of 7KC on choroid. In cultured CECs, 7KC increased mesenchymal proteins and reduced endothelial proteins, VEGFR2, CD31 and VE-cadherin. These findings support the thinking that increased 7KC in drusen and the blood stream during aging promotes EndMT of CECs and, therefore, leads to invasive MNV with vision loss and subretinal fibrosis that expresses less VEGFR2 and is less responsive to anti-VEGF treatment.

An important inducer and downstream effector of EndMT is TGFβ [42]. In pathologic conditions, inflammation, hypoxia and oxidative stress aggravate mesenchymal transitions through intricate signaling networks, involving TGFβ, Wnt-β catenin and Notch [43]. We observed TGFβ was increased in 7KC-treated CECs, and that CECs pretreated with the TGFβ receptor inhibitor, did not experience mesenchymal transition, supporting the hypothesis that 7KC-mediated EndMT of CECs involved TGFβ-regulated signaling. TGFβ signaling involves transcriptional factors that are involved in mesenchymal transition, including SMADs, or SNAIL, which have shown involved in TGFβ-mediated EMT [39]. 7KC treatment upregulated SMAD2/3 in CECs, whereas inhibition of TGFβ signaling inhibited 7KC-mediated upregulation of SMAD2/3. Knockdown of SMAD3 by siRNA, but not SMAD2, partially inhibited 7KC-mediated loss of endothelial markers and increase in mesenchymal proteins, suggesting SMAD3 may function as a transcription factor of 7KC-mediated EndMT of CECs but interacts with other factors or signaling pathways. These findings provide evidence that SMAD3 is involved in 7KC mediated CEC EndMT through TGFβ-mediated signaling.

We also tested if CECs that had undergone EndMT in response to 7KC would be more invasive and found that CECs treated with 7KC increased cell migration but failed to form cell connections. Although the tube assay does not represent the complex interactions involved in angiogenesis [44], it allowed us to determine if the transitioned cells could still form connections. We found that 7KC-treated cells lost the capacity to form connections between cells. Both outcomes support the hypothesis that 7KC induces EndMT of CECs and causes them to become invasive migratory mesenchymal cells that no longer function as endothelial cells and promote fibrosis. Activation of Rac1 is required for VEGF-mediated CEC migration [45]. Inhibition of Rac1 activation blocked cell migration induced by 7KC, supporting the hypothesis that 7KC may play a role in invasive forms of macular neovascularization in AMD as well as invasive migratory transitioned mesenchymal cells. Together, these findings suggest broader or regulatory treatments besides anti-VEGF treatment may be useful in neovascular AMD when fibrosis can be predicted.

In summary, increased 7KC in the blood of choriocapillary vessels and in Bruch's membrane during aging promotes EndMT of CECs via TGFβ-dependent SMAD3 upregulation. The mesenchymal cells derived from CECs have a greater migratory phenotype, and can lead to type 2 MNV in the neural retina, which is a leading cause of vision loss in neovascular AMD. Change of CECs to mesenchymal cells may lead to fibrosis and reduced sensitivity to anti-VEGF agents.

Supplementary Information The online version contains supplementary material available at https://doi.org/10.1007/s10456-021-09770-0.

Acknowledgments This work was supported by the National Institutes of Health EY014800 and an Unrestricted Grant from Research to Prevent Blindness, Inc., New York, NY, to the Department of Ophthalmology & Visual Sciences, University of Utah; and the National Institutes of Health R01EY015130 and R01EY017011 to M.E.H.

Author contributions HW developed the hypothesis, designed and performed the experiments and wrote the manuscript; AR and EK performed experiments, maintained the animals and reviewed the manuscript; MEH developed the hypothesis, designed the experiments, wrote the manuscript, provided funding support and oversaw lab proceedings.

Data availability The datasets generated during and/or analysed during the current study are available from the corresponding author on reasonable request.

Compliance with ethical standards

Conflict of interest The authors declared there were no conflicts of interests to disclose.

References

1. Blasiak J et al (2014) Oxidative stress, hypoxia, and autophagy in the neovascular processes of age-related macular degeneration. Biomed Res Int 2014:768026
2. Wang H, Hartnett ME (2016) Regulation of signaling events involved in the pathophysiology of neovascular AMD. Mol Vis 22:189–202
3. Evans RN et al (2020) Associations of Variation in Retinal Thickness With Visual Acuity and Anatomic Outcomes in Eyes With Neovascular Age-Related Macular Degeneration Lesions Treated With Anti-Vascular Endothelial Growth Factor Agents. JAMA Ophthalmol
4. Bhisitkul RB et al (2015) Macular atrophy progression and 7-year vision outcomes in subjects from the ANCHOR, MARINA, and HORIZON studies: the SEVEN-UP study. Am J Ophthalmol 159(5): 915-24 e2.
5. Cheung CMG et al (2019) The evolution of fibrosis and atrophy and their relationship with visual outcomes in asian persons with neovascular age-related macular degeneration. Ophthalmol Retina 3(12):1045–1055
6. Fritsche LG et al (2014) Age-related macular degeneration: genetics and biology coming together. Annu Rev Genomics Hum Genet 15:151–71
7. Seddon JM et al (2007) Association of CFH Y402H and LOC387715 A69S with progression of age-related macular degeneration. JAMA: J Am Med Assoc 297(16):1793–1800
8. Domalpally A et al (2019) Prevalence, risk, and genetic association of reticular pseudodrusen in age-related macular degeneration: age-related eye disease study 2 report 21. Ophthalmology 126(12):1659–1666
9. Merle BM et al (2016) Dietary folate, B vitamins, genetic susceptibility and progression to advanced nonexudative age-related macular degeneration with geographic atrophy: a prospective cohort study. Am J Clin Nutr 103(4):1135–44
10. Fernandez-Godino R (2018) Alterations in extracellular matrix/bruch's membrane can cause the activation of the alternative complement pathway via tick-over. Adv Exp Med Biol 1074:29–35
11. Thulliez M et al (2019) Correlations between choriocapillaris flow deficits around geographic atrophy and enlargement rates based on swept-source OCT imaging. Ophthalmol Retina 3(6):478–488
12. Lamin A et al (2019) Changes in volume of various retinal layers over time in early and intermediate age-related macular degeneration. Eye (Lond) 33(3):428–434
13. Freund KB, Zweifel SA, Engelbert M (2010) Do we need a new classification for choroidal neovascularization in age-related macular degeneration? Retina 30(9):1333–49
14. Peterson LJ et al (2007) Heterotypic RPE-choroidal endothelial cell contact increases choroidal endothelial cell transmigration via PI 3-kinase and Rac1. Exp Eye Res 84(4):737–744
15. Wang H et al (2015) Rap1 GTPase inhibits tumor necrosis factor-alpha-induced choroidal endothelial migration via NADPH oxidase- and NF-kappaB-dependent activation of Rac1. Am J Pathol 185(12):3316–25
16. Monaghan-Benson E et al (2010) The Role of vascular endothelial growth factor-induced activation of NADPH oxidase in choroidal endothelial cells and choroidal neovascularization. Am J Pathol 177(4):2091–2102
17. Monaghan-Benson E, Burridge K (2009) The regulation of VEGF-induced microvascular permeability requires Rac and ROS. J Biol Chem M109
18. Wang H et al (2011) Upregulation of CCR3 by age-related stresses promotes choroidal endothelial cell migration via VEGF-dependent and -independent signaling. Investigat Ophthalmol Visual Sci 52(11):8271–8277
19. Wang H et al (2016) Retinal inhibition of CCR3 induces retinal cell death in a murine model of choroidal neovascularization. PLoS One 11(6):e0157748
20. Anderson A et al (2020) 7-Ketocholesterol in disease and aging. Redox Biol 29:101380
21. Rodriguez IR, Larrayoz IM (2010) Cholesterol oxidation in the retina: implications of 7KCh formation in chronic inflammation and age-related macular degeneration. J Lipid Res 51(10):2847–62
22. Rodriguez IR et al (2014) 7-ketocholesterol accumulates in ocular tissues as a consequence of aging and is present in high levels in drusen. Exp Eye Res 128:151–5
23. Crabb JW et al (2020) Drusen proteome analysis: An approach to the etiology of age-related macular degeneration. Proceed Natl Acad Sci 222551899.
24. Fliesler SJ (2015) Cholesterol homeostasis in the retina: seeing is believing. J Lipid Res 56(1):1–4
25. Curcio CA et al (2001) Accumulation of cholesterol with age in human Bruch's membrane. Invest Ophthalmol Vis Sci 42(1):265–74
26. Curcio CA et al (2005) Esterified and unesterified cholesterol in drusen and basal deposits of eyes with age-related maculopathy. Exp Eye Res 81(6):731–741
27. Vejux A et al (2020) 7-Ketocholesterol and 7β-hydroxycholesterol: In vitro and animal models used to characterize their activities and to identify molecules preventing their toxicity. Biochem Pharmacol 173:113648
28. Dugas B et al (2010) Effects of oxysterols on cell viability, inflammatory cytokines, VEGF, and reactive oxygen species production on human retinal cells: cytoprotective effects and prevention of VEGF secretion by resveratrol. Eur J Nutr 49(7):435–46
29. Chakravarthy U et al (2020) Progression from early/intermediate to advanced forms of age-related macular degeneration in a large UK cohort: rates and risk factors. Ophthalmol Retina 4(7):662–672
30. Wang H et al (2020) IQGAP1 causes choroidal neovascularization by sustaining VEGFR2-mediated Rac1 activation. Angiogenesis
31. Becker S et al (2018) Targeted Knockdown of Overexpressed VEGFA or VEGF164 in Muller cells maintains retinal function by triggering different signaling mechanisms. Sci Rep 8(1):2003
32. Li W et al (2011) Lipid accumulation and lysosomal pathways contribute to dysfunction and apoptosis of human endothelial cells caused by 7-oxysterols. Biochem Biophys Res Commun 409(4):711–6
33. Inagaki S et al (2020) Anti-vascular endothelial growth factor antibody limits vascular leakage and decreases subretinal fibrosis in a cynomolgus monkey choroidal neovascularization model. Curr Neurovasc Res
34. Shu DY, Butcher E, Saint-Geniez M (2020) EMT and EndMT: emerging roles in age-related macular degeneration. Int J Mol Sci 21(12)

35. Alyaseer AAA, de Lima MHS, Braga TT (2020) The role of NLRP3 inflammasome activation in the epithelial to mesenchymal transition process during the fibrosis. Front Immunol 11:883
36. Radeke MJ et al (2015) Restoration of mesenchymal retinal pigmented epithelial cells by TGFbeta pathway inhibitors: implications for age-related macular degeneration. Genome Med 7(1):58
37. Bischoff J (2019) Endothelial-to-mesenchymal transition. Circ Res 124(8):1163–1165
38. Schmierer B, Hill CS (2007) TGFbeta-SMAD signal transduction: molecular specificity and functional flexibility. Nat Rev Mol Cell Biol 8(12):970–82
39. Syed V (2016) TGF-β signaling in cancer. J Cell Biochem 117(6):1279–87
40. Gurzu S et al (2019) Epithelial mesenchymal and endothelial mesenchymal transitions in hepatocellular carcinoma: a review. Biomed Res Int 2019:2962580
41. Rossato FA et al. (2020) Fibrotic changes and endothelial-to-mesenchymal transition promoted by VEGFR2 antagonism alter the therapeutic effects of VEGFA pathway blockage in a mouse model of choroidal neovascularization. Cells 9(9).
42. Piera-Velazquez S, Jimenez SA (2019) Endothelial to mesenchymal transition: role in physiology and in the pathogenesis of human diseases. Physiol Rev 99(2):1281–1324
43. Souilhol C et al (2018) Endothelial-mesenchymal transition in atherosclerosis. Cardiovasc Res 114(4):565–577
44. Nowak-Sliwinska P et al (2018) Consensus guidelines for the use and interpretation of angiogenesis assays. Angiogenesis 21(3):425–532
45. Wang H et al (2011) The role of RPE cell-associated VEGF189 in choroidal endothelial cell transmigration across the RPE. Investigat Ophthalmol Visual Sci 52(1):570–578